Numerical modelling of transient cyclic vertical loading of suction caissons in sand

Cerfontaine, Benjamin; Collin, Frédéric; Charlier, Robert

Published in:
Geotechnique

DOI:
10.1680/jgeot.15.P.061

Publication date:
2016

Document Version
Publisher's PDF, also known as Version of record

Cerfontaine, B. *et al*. (2016). *Géotechnique* **66**, No. 2, 121–136 [http://dx.doi.org/10.1680/jgeot.15.P.061]

Numerical modelling of transient cyclic vertical loading of suction caissons in sand

B. CERFONTAINE*, F. COLLIN* and R. CHARLIER*

This paper presents numerical investigations of the monotonic and cyclic behaviours of suction caissons upon vertical transient loading. Both drained and partially drained conditions are investigated. Monotonic compression and traction simulations are carried out to qualitatively compare results with the literature and validate the model. They highlight the different modes of reaction of the caisson to both compression and traction loading. A sensitivity analysis points out the strong influence of some parameters on the resistance of the caisson but also on the failure mechanism. The transient behaviour of the caisson upon different kinds of cyclic load signals is analysed. Results reproduce the settlement and pore water pressure accumulations observed during experiments. The influence of the key design parameters on the settlement accumulation is also assessed. Finally a cyclic diagram is proposed to describe the evolution of the final settlement upon different magnitudes of loading.

KEYWORDS: finite-element modelling; offshore engineering; repeated loading; sands; soil/structure interaction

INTRODUCTION

Nowadays the demand for renewable energy in the European Union (EU) is strongly increasing following the EU climate and energy package targets for 2020. The final compromise plans

(*a*) 20% reduction of EU greenhouse gas emissions from 1990 levels
(*b*) 20% of the EU energy consumption produced from renewable resources
(*c*) 20% improvement in the EU's energy efficiency.

In this context, offshore power plants represent an attractive eco-friendly source of electric power. The total capacity of wind turbines across the EU was 5 GW at the end of 2012, mainly in the UK, but is expected to reach 40 GW by 2020 and 150 GW by 2030 (Corbetta *et al.*, 2014). Foundation design is a crucial issue to ensure the economic viability of offshore power plant projects. Indeed their costs may represent up to a third of the total cost (Byrne & Houlsby, 2003; Senders, 2008). Moreover, wind farms are built further away from the coast and in deeper waters, increasing technical challenges for designers. Additional environmental constraints, such as noise emissions in the case of pile driving, could also be added to the technical requirements (Thieken *et al.*, 2014). Therefore, there is a real need for innovative foundation techniques and design procedures.

Among different types of foundations, suction caissons, also termed bucket foundations or suction anchors, should be highlighted (Iskander *et al.*, 2002; Houlsby *et al.*, 2005a). They consist of a hollow cylinder open towards the bottom. Their top (the lid) can be a stiffer plate or a dome (Tran, 2005). The idea of a suction anchor is not new and arose in the 1960s (Goodman *et al.*, 1961) to replace inefficient weight anchors. They were mainly used as temporary anchorages (Senpere & Auvergne, 1982). The first structures employing the system as permanent foundations in clay or sand were built in the early 1990s (Tjelta *et al.*, 1990).

Installation of suction caissons is straightforward and does not require heavy equipment (Houlsby & Byrne, 2005). Initially the caisson penetrates the sea bed under its own weight. Water trapped inside is allowed to escape through an opening. It is pumped out afterwards, creating a differential of fluid pressure between inside and outside, as shown in Fig. 1. This differential of pressure digs the caisson into the soil. The created seepage flow reduces the penetration resistance at the tip and along the inner skirt, facilitating the installation (Senders & Randolph, 2009).

The suction caisson concept covers distinct realities of geometries, soil conditions and behaviours. If the superstructure is a monopod – that is, there is a single foundation for a wind turbine – the main loading is a combination of overturning moment, horizontal and vertical loads (Byrne & Houlsby, 2004; Achmus *et al.*, 2013). If the superstructure is a multipod – that is, the wind turbine is supported by several foundations – the overturning moment is mainly transformed into a push–pull loading of the suction caissons (Senders & Randolph, 2009).

Structures for offshore wind turbines are light but subjected to a large overturning moment. Therefore, the behaviour of the caisson under a large extraction load is one of the main issues (Houlsby *et al.*, 2005b, 2006; Gao *et al.*, 2013). Interfaces play a crucial role in the mobilisation of the caisson's resistance (Achmus *et al.*, 2013; Kourkoulis *et al.*, 2014). Moreover it is proven that under a large traction load, a suction effect similar to the installation process balances the loading. However, this effect is purely transient and depends on many parameters such as permeability, geometry of the caisson, rate of loading, and so on. The question of whether this behaviour should be taken into account or not in the design is still open.

The cyclic nature of the loading complicates the problem, since the behaviour of sand in this case is quite complex. It is widely studied in the fields of earthquake (Alarcon-Guzman *et al.*, 1988; Ishihara, 1996; Hyodo *et al.*, 2002) and offshore geotechnics (Rahman *et al.*, 1977). The main outcome is the pore water pressure (PWP) and settlement accumulations

Manuscript received 1 April 2015; revised manuscript accepted 9 September 2015. Published online ahead of print 20 November 2015.
Discussion on this paper closes on 1 July 2016, for further details see p. ii.
* University of Liege, Geomechanics and Engineering Geology, Liege, Belgium.

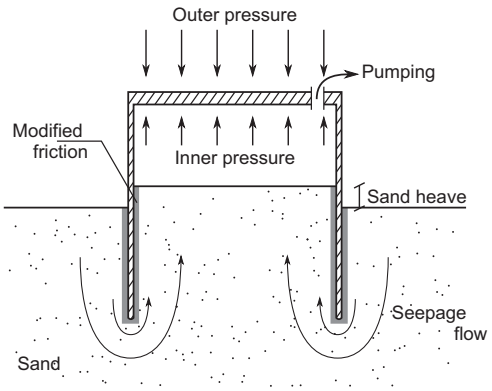

Fig. 1. Sketch of the installation process

with increasing number of cycles. This general behaviour is also observed for suction caissons experimentally (Byrne & Houlsby, 2004; Kelly *et al.*, 2006a, 2006b; Zhu *et al.*, 2013) and numerically (Cerfontaine *et al.*, 2014, 2015a). Therefore, the modelling of this sand behaviour requires specific constitutive laws.

This paper presents numerical drained and partially drained simulations of monotonic and cyclic loadings of a suction caisson embedded in dense sand upon vertical loading. Comparisons with experiments are mainly qualitative due to the lack of published data. They refer to published papers on experiments and numerical simulations. A state of the art is provided by Thieken *et al.* (2014). Sensitivity analyses are carried out on main parameters. The first objective is the deep understanding of the different mechanisms of resistance of the caisson upon monotonic loading and their interactions. The second objective is to understand the cyclic behaviour of suction caissons in the light of their monotonic response. The evolution of the settlement with time is investigated in particular. Finally, a cyclic diagram is elaborated to facilitate pre-design of foundations and this highlights the influence of loading parameters. The level of cyclic loading is kept limited in order to avoid failure and merely focuses on the evolution of settlement (serviceability) rather than global resistance.

The first part of this paper describes the numerical model. Geometry, boundary conditions and elaboration of the cyclic loading signal are defined. The main two numerical tools, namely the constitutive law of the soil and an interface finite element are briefly introduced. The second part focuses on the monotonic behaviour of a suction caisson in drained or partially drained conditions and the influence of the main parameters. The last part extends the conclusions of the previous part to understand the phenomena involved in the cyclic loading of a caisson.

NUMERICAL MODEL

Geometry

A sketch of the investigated suction caisson is provided in Fig. 2. The studied behaviour is purely vertical so the mesh is axisymmetric. The cross-section of the caisson is assumed to be circular. The diameter D of the caisson is equal to 7·8 m and its length L is 4 m.

The caisson is made of a stiff lid (0·4 m thick), closing its upper aperture, and a more flexible skirt (0·1 m thick). The thickness to diameter ratio is equal to 1·2%, but ranges between 0·3 and 0·6% for actual geometries (Byrne & Houlsby, 2002; Kelly *et al.*, 2006b; Tran, 2005). It is greater than for actual caissons for numerical purposes. Indeed, this avoids the use of very thin elements within the mesh of the caisson and mesh disturbances.

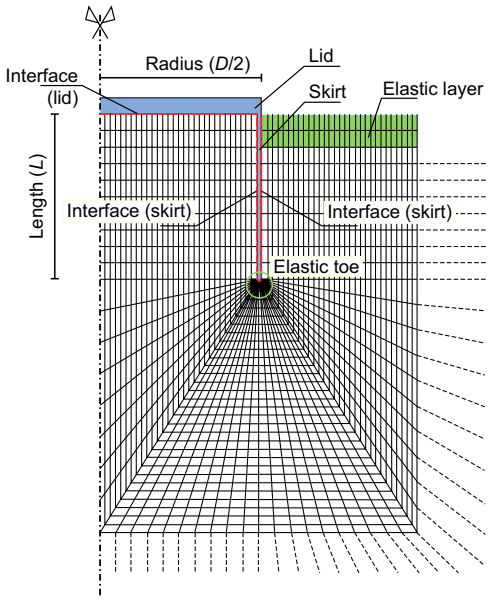

Fig. 2. Mesh adopted around the caisson

The behaviour of sands is inherently non-linear and involves plasticity effects such as contractancy and dilatancy. Therefore, elastic models are not sufficient. Classical elasto-plastic models are able to reproduce the monotonic behaviour of sands, but not the cyclic behaviour, involving plasticity during loading and unloading. The adopted Prevost model is described in the following.

The superficial sand layer outside the caisson is prone to liquefaction due to its low confinement. However, modelling its post-liquefaction is meaningless within the scope of this study since it does not contribute significantly to the resistance of the foundation. It is modelled by a linear elastic soil layer. The depth of this layer is limited to 0·8 m. It includes the first two rows of elements. Similarly, an elastic toe is also set up under the tip of the caisson, as shown in Fig. 2. It compensates the overestimated width of the skirt.

The soil is assumed to be a very dense sand (relative density of 90%). The specific weight of the solid grains is equal to 26·5 kN/m^3, the porosity of the soil is 0·36 and its permeability is 5×10^{-12} m^2 (corresponding to 5×10^{-5} m/s) (Andersen *et al.*, 2008).

The 26 m $\times$ 24 m mesh is composed of 2364 hydro-mechanical coupled finite elements and 7085 nodes. A description of these elements can be found in Gerard *et al.* (2008). Hydro-mechanical interface elements are set up between the soil and the caisson. The installation phase of the suction caisson is not considered.

Boundary conditions

The lower limit of the mesh is deemed impervious, that is, it corresponds to a layer of consolidated clay under the sand layer, for example. The right and upper sides of the mesh are considered drained. They correspond, respectively, to the continuity of the sand layer and to the transition between the sand layer and the sea.

Initial stresses

The sea level is considered to be 10 m over the sand layer. It is taken into account by a vertical pressure of 100 kPa applied at the top of the soil, as represented in Fig. 3. The corresponding initial PWPs are set up accordingly in the whole domain. Effective stresses are initialised within

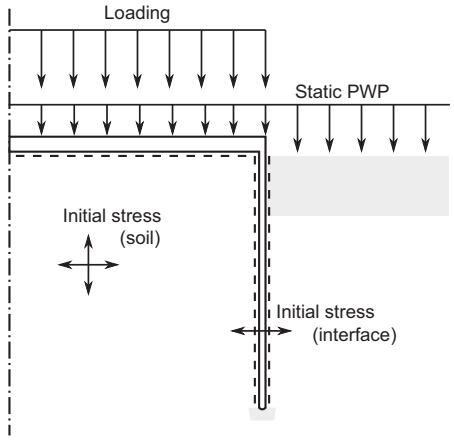

Fig. 3. Sketch of loading applied to caisson and initial stresses

the soil (and the interface), due to its self-weight. The coefficient of earth pressure at rest, K_0, is assumed as equal to 1.

Loading of the caisson

The loading of the caisson consists of a stress-controlled signal applied at the top of the lid, as shown in Fig. 3. Monotonic loading is simply a positive (compression) or negative (traction) pressure applied uniformly at a constant rate. The cyclic loading is a more complex pressure signal and is described in the following.

Constitutive laws

Elastic zones. The elastic toe and the superficial elastic layer are assumed to have a linear behaviour. The elastic parameters of the elastic layer are equal to $(E, \nu) = (10\ \text{MPa}, 0{\cdot}15)$. They are chosen one order of magnitude lower than elastic parameters of the elasto-plastic model. The choice of parameters for the elastic toe is described later. The caisson is made of steel and assumed to remain elastic-linear. Its parameters are equal to $(E, \nu) = (200\ \text{GPa}, 0{\cdot}3)$.

Prevost model. The Prevost model (Prevost, 1985; Yang *et al.*, 2003) is adopted because of its physically based concept. Its parameters are obtained from classical monotonic and cyclic triaxial tests. It is able to reproduce the salient features of the cyclic behaviour of cohesionless soils.

This model belongs to the multi-surface family (Dafalias & Popov, 1975; Prevost, 1977). The evolution of plastic modulus is discretised through a finite number of nested hardening surfaces f^i, as shown in Fig. 4. They read

$$f^i \equiv \left[\boldsymbol{s} - (p' + p_c)\,\boldsymbol{\alpha}^i\right] : \left[\boldsymbol{s} - (p' + p_c)\,\boldsymbol{\alpha}^i\right] - \frac{2}{3}\left[(p' + p_c)\,M^i\right]^2 = 0 \tag{1}$$

where $\boldsymbol{s}$ is the deviatoric part of the effective stress tensor $\boldsymbol{\sigma}'$, p' is the mean effective stress, p_c is the shift of the apex of the surfaces along the p-axis taking cohesion into account, $\boldsymbol{\alpha}$ is a back-stress tensor defining the position of the yield surface in the stress space, M^i is the aperture of the surface and ':' is the dot product.

The plastic component of the variation of volumetric strains $\dot{\varepsilon}_v^p$ reads

$$\dot{\varepsilon}_v^p = \dot{\lambda}\,\frac{1}{3}\,\frac{\bar{\eta}^2 - \eta^2}{\bar{\eta}^2 + \eta^2} \quad \text{if} \quad \dot{\lambda} > 0 \tag{2}$$

where $\eta = q/p' + p_c$, q is the invariant of the deviatoric stress tensor and $\dot{\lambda}$ is the variation of plastic multiplier obtained

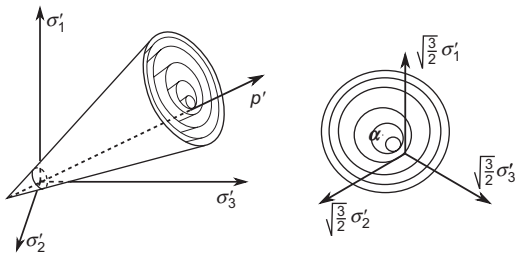

Fig. 4. Nested surfaces in the principal stress space

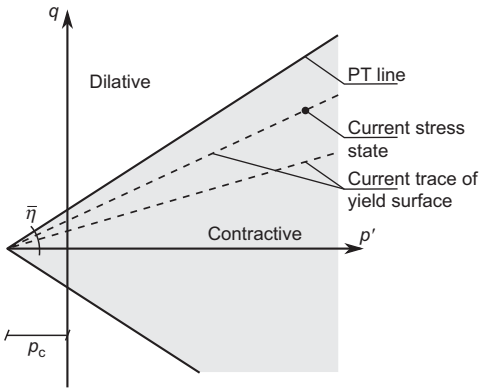

Fig. 5. Non-associated plastic potential of Prevost model

through the consistency condition. Equation (2) introduces the parameter $\bar{\eta}$ corresponding to the phase transformation line (Ishihara, 1996). Such a formulation divides the p'–q plane into two zones of either contractive or dilative plastic behaviours, as shown in Fig. 5.

An evolution of the stiffness parameters with confinement is introduced, for instance the shear modulus reads

$$G(p') = G_{\text{ref}}\left(\frac{p'}{p_{\text{ref}}}\right)^{0{\cdot}5} \tag{3}$$

where G_{ref} is a reference modulus and p_{ref} is a reference pressure, equal to atmospheric pressure in this case. This relation can be extended to the bulk modulus K and to the field of plastic moduli H^i discretised by the nested surfaces.

A full description of the model implementation into the finite-element code LAGAMINE and calibration of parameters can be found in the thesis by Cerfontaine (2014). These parameters correspond to a very dense Lund sand (Ibsen & Jacobsen, 1996). Elastic stiffness parameters are equal to $(K_{\text{ref}}, G_{\text{ref}}) = (65, 47)$ MPa. The phase transition line slope $\bar{\eta}$ is equal to 1·15 and the cohesion shift p_c to 5 kPa.

Interface elements

The hydro-mechanical finite element of interface implemented in the LAGAMINE code encompasses two distinct but coupled problems, as extensively described in Cerfontaine *et al.* (2015b). The first one is the mechanical contact problem, involving detection of contact, shearing or sliding. The second problem deals with the water flow through and along the interface.

The interface finite elements belong to the zero-thickness family. They discretise the probable zone of contact and are activated only in this case (Goodman *et al.*, 1968; Habraken *et al.*, 1998). The ideal contact constraint states that

$$g_N \geq 0, \quad p'_N \geq 0 \quad \text{and} \quad p'_N\,G_N = 0 \tag{4}$$

where p'_N is the effective contact pressure and g_N is the gap between both sides of the interface, as shown in Fig. 6(a). This ideal constraint establishes that contact holds if the gap is equal to zero (closed), giving rise to a normal contact pressure. Otherwise, if the gap is positive (open), there is no contact pressure. This constraint is numerically enforced by a penalty method leading to

$$\dot{p}'_N = -K_N \dot{g}_N \tag{5}$$

where K_N is a penalty coefficient. In this case, the gap becomes negative, that is, the contact pressure develops if there is an interpenetration of the solids. Contact is lost when the effective pressure is equal to zero. It cannot be negative in order to prevent traction of the solid skeleton of the sand.

The shear behaviour of the interface is described similarly. The ideal tangential behaviour distinguishes between stick and sliding states (Wriggers, 2006). In the former state, the shear stress is different from zero but the relative tangential displacement is null. In the second state, the stress state is bounded to τ_{max}, but there is a relative displacement. Once again, the ideal relation is regularised by a penalty method and the evolution of the shear stress τ within the interface reads

$$\dot{\tau} = K_T \dot{g}_T \tag{6}$$

where $\dot{g}_T$ is the variation of tangential displacement and K_T is the tangential penalty coefficient. The maximum shear stress τ_{max} is bounded by a Coulomb criterion according to

$$\tau_{max} = \mu p'_N \tag{7}$$

where μ is the friction coefficient of the interface.

Interfaces represent a preferential path for the fluid flow (Gens *et al.*, 1988). In this work, both fluid flow through and along the interface are taken into account, as illustrated in Fig. 6(b). A three-node discretisation of the field of pressures is adopted. It is discretised by nodes on each side of the interface and inner nodes, as shown in Fig. 6(b). Therefore, each transversal flow between one side of the interface and inside depends on the transversal drop of pressure Δp_w such that

$$f_{wt} = \rho_w T_w \Delta p_w \tag{8}$$

where ρ_w is the specific mass of the fluid and T_w is a transversal conductivity. The longitudinal water flow f_{wl} depends on the longitudinal gradient of water pressure ∇p_w inside such that

$$f_{wl} = -\rho_w \frac{k_l}{\mu_w} (\nabla p_w + \rho_w g \nabla z) \tag{9}$$

where $\rho_w g \nabla z$ is the static pressure gradient, k_l is the longitudinal permeability and μ_w is the dynamic viscosity of water.

The first coupling between mechanical and flow problems proceeds from the definition of a total pressure p_N acting on each side of the interface according to the Terzaghi's principle

$$p_N = p'_N + p_w \tag{10}$$

where p_w is the fluid pressure computed on the inner nodes of the interface element. The second coupling arises from the variation of longitudinal permeability with respect to the gap aperture. If the gap is opening, longitudinal permeability is assumed to vary according to the cubic law (Segura & Carol, 2008)

$$k_l = \frac{(g_N)^2}{12} \tag{11}$$

Finally, the progressive opening or closure of the gap saturated with water implies the variation of the stored mass of water. Assume two plane surfaces of unit area A separated by a gap g_N, the variation of the fluid mass $\dot{M}_f$ due to a variation of the gap or fluid density reads

$$\dot{M}_f = (\rho_w \dot{g}_N + \dot{\rho}_w g_N) A \tag{12}$$

The parameters adopted hereafter are provided in Table 1.

Table 1. Parameters of the interface

μ	K_N: N/m^{-3}	K_T: N/m^{-3}	T_w: (m/Pa)/s
0·5	10^{10}	10^{10}	10^{-3}

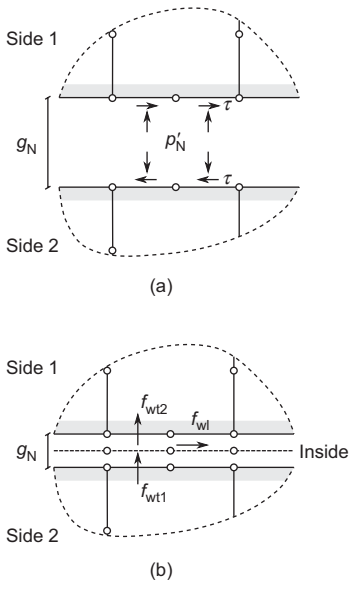

Fig. 6. Discretisation of the finite element of interface

MONOTONIC LOADING

Two configurations of monotonic loading are considered: drained and partially drained. In the former, the loading rate is assumed to be very slow with respect to the PWP dissipation rate within the soil. Therefore, the PWPs remain equal to their initial value. In the second case, the PWPs generated diverge from their initial values. However, the simulation is not undrained and they are able to dissipate progressively.

A positive or negative variation of vertical load applied to the caisson is balanced by different components of reaction, described in Fig. 7. The variation of total load applied on the upper part of the lid of the caisson is termed ΔF_{tot}. The integral of the variation of PWP distribution on the lower part of the lid of the caisson is represented by ΔF_{pw}. The integral of the effective contact stresses on this lower part is gathered into ΔF_{lid}. The integral of the variation of shear stresses along the skirt of the caisson is denoted ΔF_{in} inside and ΔF_{out} outside. In the following they are depicted with respect to the displacement of the top centre of the caisson Δy.

Stress-controlled simulations are carried out up to the local failure of a material point or to the global failure of the soil–caisson system. The post-failure behaviour of the system of foundations is not represented. Thus the maximum displacement remains limited.

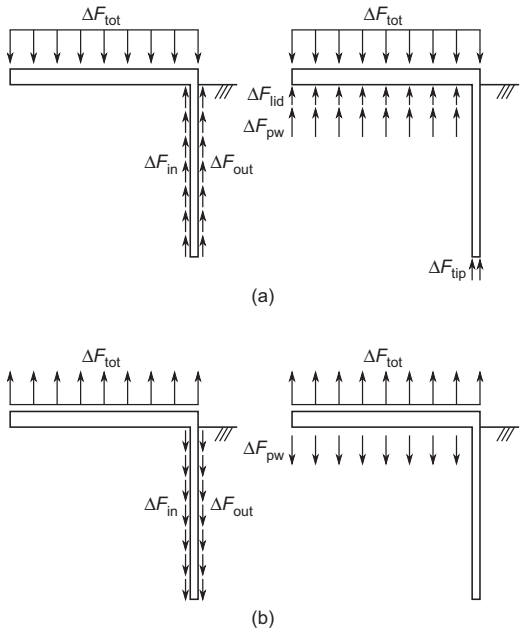

Fig. 7. Comparison of reaction components: (a) compression load, ΔF_{tot}; (b) traction load, ΔF_{tot}

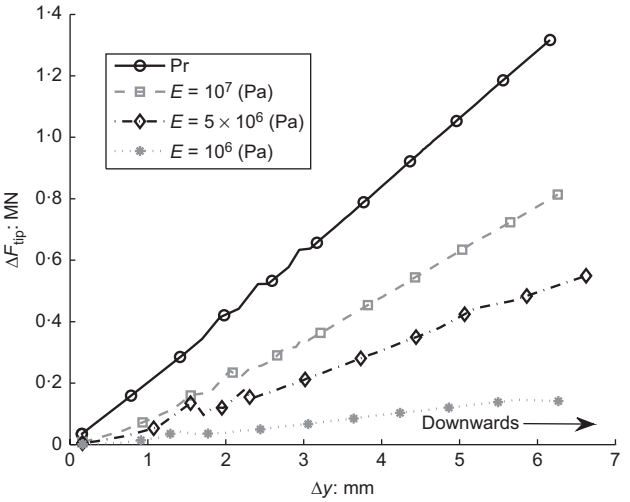

Fig. 8. Comparison of the reaction component sustained by the tip of the caisson for different configurations of the elastic toe: Pr stands for Prevost model and *E* denotes the Young's modulus of the purely elastic toe, drained compression simulation

Characterisation of the elastic zones

The elastic toe under the tip of the caisson has two main purposes: to avoid failure of the soil due to the very large stress concentration and to compensate for the too-large width of the caisson skirt. It was stated before that the area of the tip is overestimated by a factor between two and four with respect to the classical thickness-to-diameter ratio. Therefore, the Young's modulus should be chosen in order to reduce the load balanced by the tip.

The reaction component sustained by the tip of the caisson is illustrated in Fig. 8 in the case of a drained compression simulation. The response of the caisson where the toe is described by the same elastoplastic model as the surrounding soil (termed Pr for Prevost model) is compared with solutions for varying Young's moduli (E). The adopted solution should lie between the 10^6 Pa and 10^7 Pa simulations to correspond to an acceptable reduction factor. Considering a Young's modulus equal to 5×10^6 Pa decreases the component of reaction by a factor of 2·5 and this is adopted in the following.

On the contrary, the variation of the elastic modulus of the elastic superficial layer hardly affects the results and is not represented here. The choice of a Young's modulus equal to 1×10^7 Pa leads to the closest fit of the purely elastoplastic model.

Compression simulations

Drained configuration. Drained results upon compression load are provided in Figs 9(a) and 9(b). The simulation underlines the sequential mobilisation of the reaction components.

Initially the main part of the loading ΔF_{tot} is sustained by the shear stress along the outer interface ΔF_{out}, as shown in Fig. 9(b). The share of this component is constantly decreasing as friction is progressively mobilised over the whole outer skirt, due to an excessive relative soil–caisson displacement. Finally, the value that ΔF_{out} reaches is almost constant in Fig. 9(a). It slightly increases due to the confinement rise.

The compression load ΔF_{lid} transferred by the lid to the soil plug induces a settlement, as depicted in Fig. 10(a). The first consequence is the limited soil plug–caisson relative

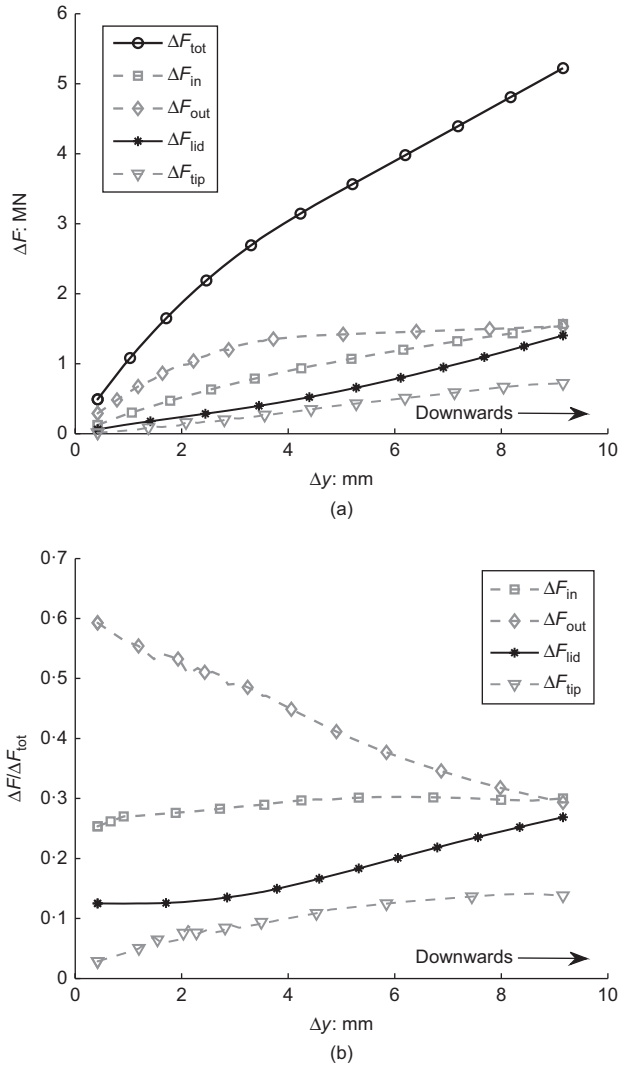

Fig. 9. Drained compression simulation: (a) variations of global reaction components; (b) variations of global reaction components to variation of total load

displacement, since they settle together. The second consequence is the increase of the confinement inside the caisson. Therefore, the inner shear stress available along the skirt ΔF_{in} is increased.

The skirt acts as a support for the lid. At the beginning the share of the lid ΔF_{lid} is only 12% of the total load, as shown in Fig. 9(b). The increase of the tip component ΔF_{tip} is larger than the increase of the lid component. However, as friction is progressively mobilised along the skirt and the soil under the tip plastifies, the stiffness of the skirt tip decreases. Thereafter the lid share starts increasing significantly.

Partially drained configuration. A partially drained compression simulation is illustrated in Fig. 11. The total load is increased up to 4·3 MN at a rate of 0·4 MN/s and kept constant afterwards. Results illustrate the increased stiffness and resistance of the caisson with respect to the drained conditions, but also highlight the transient nature of this gain.

The loading compression of the suction caisson is nothing but a classical consolidation process. However, contrary to shallow foundations, the variations of PWP are 'trapped' inside the caisson due to its skirt, limiting their dissipation. The variation of the field of PWPs generated within the soil upon a compression load is illustrated in Fig. 12. The difference of pressure between inside the caisson and outside it is at the origin of ΔF_{pw}.

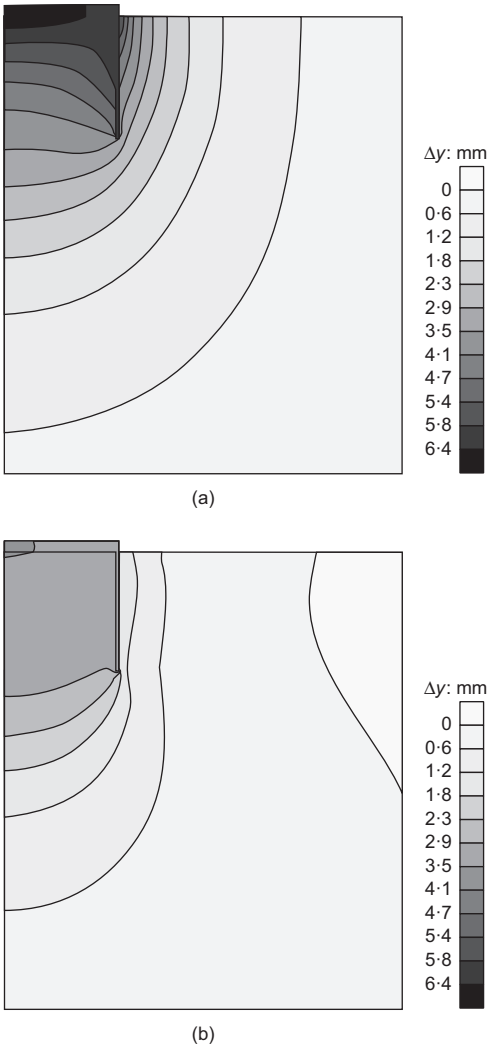

Fig. 10. Comparison of settlement of caisson and surrounding soil for $\Delta F_{tot} = 4{\cdot}3$ MN

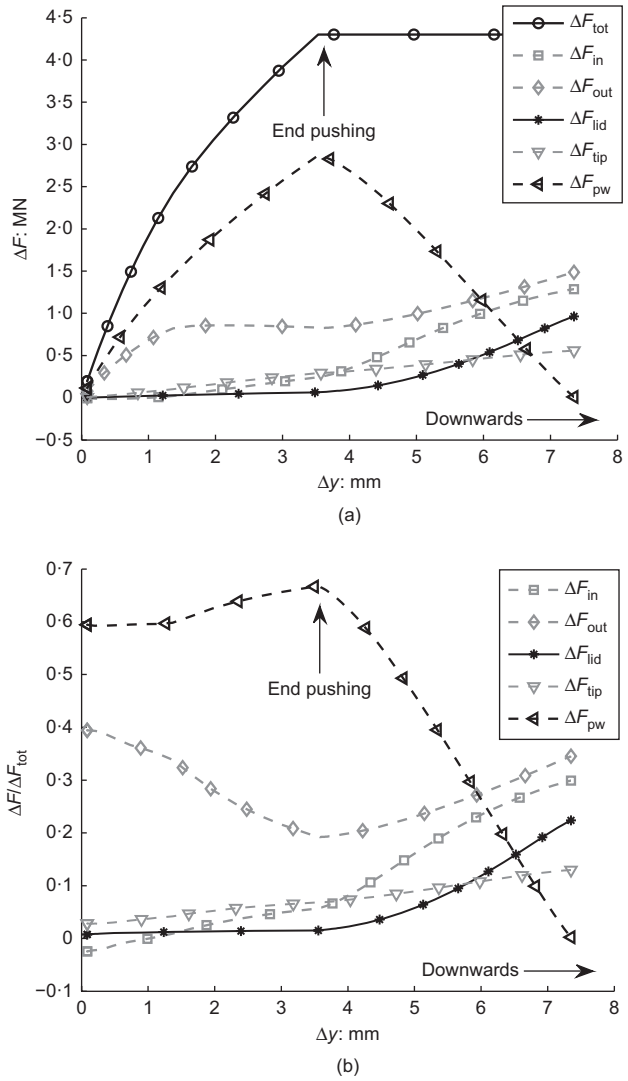

Fig. 11. Partially drained compression simulation, $k = 5 \times 10^{-12}$ m^2, rate of loading 0·4 MN/s: (a) variations of global reaction components; (b) variations of global reaction components to variation of total load

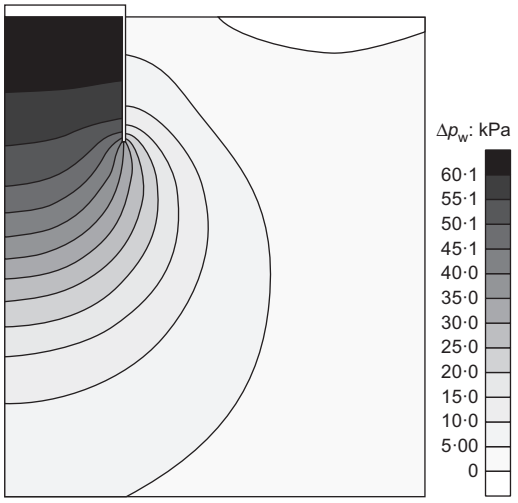

Fig. 12. Variation of pore water pressure in the soil surrounding the caisson upon compression, partially drained case, $\Delta F_{tot} = 4{\cdot}3$ MN, $k = 5 \times 10^{-12}$ m^2, rate of loading 0·4 MN/s

Similarly to the drained simulation, the share of the outer skin friction ΔF_{out} in the total resistance is continuously decreasing up to the end of the pushing phase. This component is fully mobilised and a plateau is reached (between 2 mm and 4 mm), as shown in Fig. 11(a). At the end of the pushing phase, its value is lower than in the drained simulation described in Fig. 9(a). This is due to the generation of PWP in the surrounding soil, decreasing the effective normal stresses within the soil–caisson interface. However, it increases again during the dissipation phase at constant load and recovers the drained resistance corresponding to a total load applied of 4·3 MN.

Another consequence of the PWP increase is that inner friction ΔF_{in}, tip ΔF_{tip} and lid ΔF_{lid} components do not represent a significant share of the total reaction. Indeed the behaviour of the soil plug is almost undrained. The lid ΔF_{lid} and inner shear stress ΔF_{in} components tend to zero during the pushing phase. The soil plug settles almost monolithically with the caisson, as illustrated in Fig. 10(b).

At the end of the pushing phase, the PWP variations dissipate and the fluid pressure component ΔF_{pw} is progressively dispatched between shear, lid and tip components. This illustrates that the increase of resistance can only be mobilised against a transient load.

Traction simulations

In Fig. 13(a), the pull drained simulation illustrates that only the two components of friction, ΔF_{in} and ΔF_{out}, actively contribute to the resistance to traction. The variation of ΔF_{tip} is only due to the deconfinement of initial stresses and does not play an active role in the resistance. The contact is lost under the lid and effective traction stresses are not admissible. Therefore, the lid component ΔF_{lid} is equal to zero.

The difference of stiffness between inner and outer friction components proceeds from the uplifting movement of the soil inside the caisson. The relative soil–caisson displacement is reduced and so is the shear stress mobilisation. The outer friction is fully mobilised after an upward movement of 2·5 mm and a plateau is reached in Fig. 13(a). Therefore, the increasing load is sustained only by the mobilisation of shear stress within the inner interface. Simulation stops when it is fully mobilised and no additional load can be sustained.

The partially drained simulation depicted in Fig. 13(b) illustrates the increase of resistance obtained by considering the fluid flow surrounding the caisson. Indeed, if the loading rate of the caisson is equal to 0·4 MN/s, the total load sustained for a displacement of 1·5 mm is increased by almost 50%. This phenomenon is supported by experimental (Byrne & Houlsby, 2002; Iskander *et al.*, 2002; Kelly *et al.*, 2006b) and numerical (Lehane *et al.*, 2014; Thieken *et al.*, 2014) evidence. These papers report fluid pressure components ΔF_{pw} sustaining substantially more than 50% of the total traction load applied. The negative variations of fluid pressure increase the normal effective stress within the soil–caisson interface and then the maximum friction available. The absolute value of ΔF_{out} is slightly greater than in drained conditions.

The cavitation phenomenon is not taken into account. In fact, it could be crucial, particularly during large uplift simulations, because very negative variations of pore pressure could be encountered, as observed by Byrne & Houlsby (2002) and Kelly *et al.* (2006b). However, in this case study, the sea level is assumed sufficiently high to avoid such an issue, especially within the scope of limited uplift displacements.

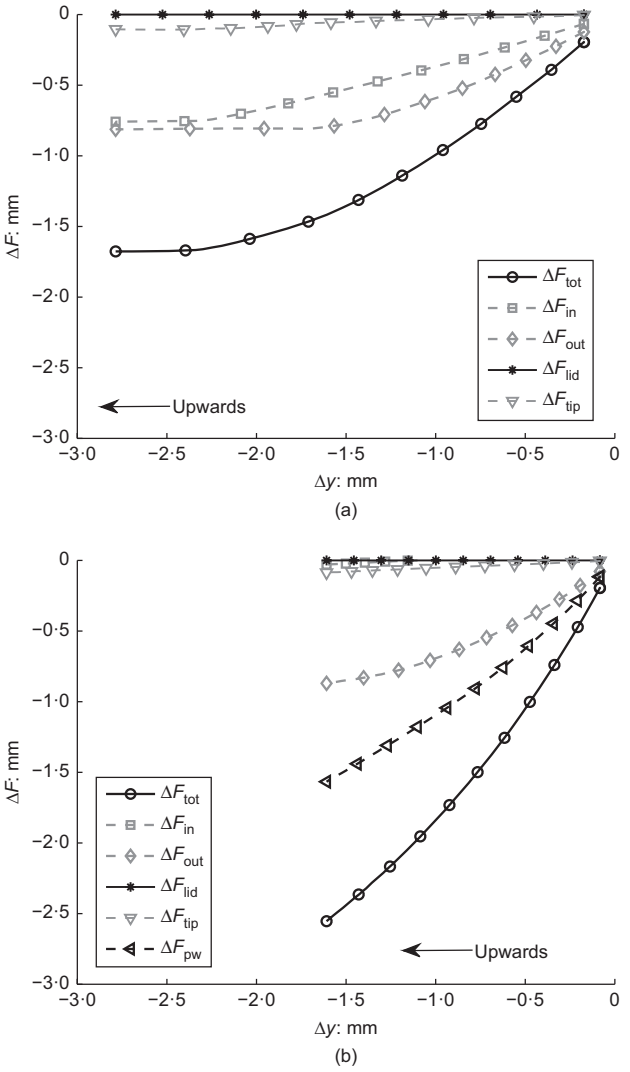

Fig. 13. Variations of global reaction components, traction simulation: (a) drained simulation; (b) partially drained simulation, $k = 5 \times 10^{-12}$ m^2

Influence of main parameters

Many strongly coupled physical phenomena are involved during the loading of suction caissons. Therefore, it is not simple to relate a single phenomenon to a given parameter, becausee they are all intricate. This section focuses on the main parameters influencing the response of the soil–caisson system.

Constitutive model and permeability of the soil. Simulations carried out for three orders of magnitude of permeability and two different constitutive laws (elastic linear or Prevost model) are illustrated in Fig. 14. For a given permeability, the divergence between the results is much stronger in compression than in traction. Indeed the constitutive law affects the stiffness of the soil, influencing ΔF_{lid} and ΔF_{tip} only activated in compression. Upon traction, friction is the main component of reaction and does not directly depend on the soil model. This reduces the difference between the Prevost and elastic models. The stiffness also degrades with increasing permeability. Indeed as dissipation rate increases, the ΔF_{pw} component is less mobilised.

A traction simulation corresponding to a higher permeability equal to $k = 5 \times 10^{-11}$ m^2 is presented in Fig. 15. The simulation starts from a positive compression load ΔF_{tot},

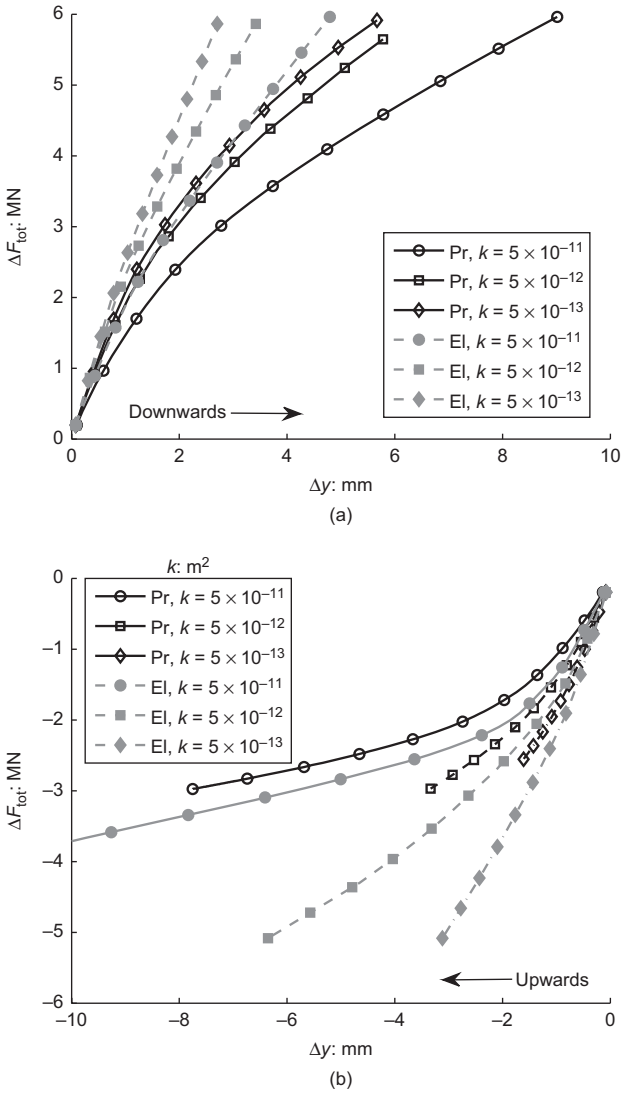

Fig. 14. Influence of the model (El for elastic linear or Pr for Prevost) and the permeability (three orders of magnitude, $k = 5 \times 10^{-11}$, 5×10^{-12}, or 5×10^{-13} m^2) on partially drained results, pull rate 0·4 MN/s: (a) compression simulation; (b) traction simulation

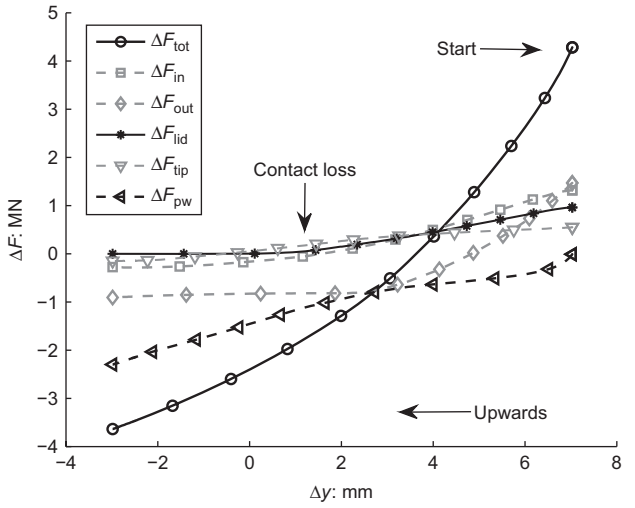

Fig. 15. Variations of global reaction components, traction partially drained simulation, $k = 5 \times 10^{-11}$ m^2

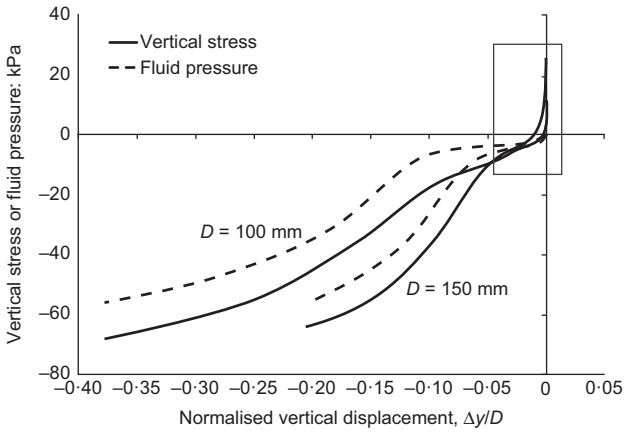

Fig. 16. Experimental results from two large-displacement pull tests described in Byrne & Houlsby (2002)

resulting from a drained compression performed up to 4·3 MN.

The behaviour of the caisson is more drained than the reference case since the permeability is higher. The PWP variation ΔF_{pw} developed is lower. There is also a larger variation of inner shear stress ΔF_{in}.

This simulation illustrates that the evolution of the PWP within the caisson, and then ΔF_{pw}, derives from different mechanisms. At the beginning, the evolution of ΔF_{pw} is quite flat. Its decrease corresponds to the consolidation process due to the reduction of confinement inside the caisson. The process is speeded up as friction is progressively mobilised along the outer part of the skirt.

From $\Delta y = +2$ mm, the PWP suddenly decreases to an almost constant rate. This proceeds from the loss of contact between the lid and the soil, indicated by a null lid component ΔF_{lid}. The opening gap under the lid acts as a piston. The decreasing PWP is due to the filling of the gap.

Figure 16 presents experimental results of a large pull test on a 79% dense Baskarp cyclone sand, described in Byrne & Houlsby (2002). The evolution of the total load ΔF_{tot} and pore pressure coefficient ΔF_{pw} can be compared qualitatively to Fig. 15. However, this comparison must be made cautiously since the material, the loading history, the permeability of the soil and so on, are different. Moreover numerical results presented here focus only on limited displacements and only the beginning of the results, as framed in Fig. 16, are pertinent for purposes of comparison.

Both numerical and experimental results present a continuous decrease of stiffness along with the increase in pull load. This reduction of the stiffness on the traction part is also observed in Kelly *et al.* (2006b). All components of reaction except ΔF_{pw} actually reach a bounded final value, as shown in Fig. 15; that is, there is no hardening or only slight hardening.

Furthermore, the shapes of the ΔF_{pw} components are quite similar in both numerical and experimental results. The experimental results also present first a relatively flat evolution, followed by a stronger rate of decrease. Despite the final displacement of the numerical simulation being limited, it shows a tendency towards the strongly decreasing PWP, as observed in the experimental results.

Loading rate. The loading rate was proven to have a strong effect on the behaviour of the caisson as observed experimentally by Senders (2008). However the influence of the loading rate can be deduced from the influence of permeability. Indeed they both affect the ratio between the rate of PWP variation and PWP dissipation. A higher loading rate induces a more undrained behaviour, which is similar to a lower permeability.

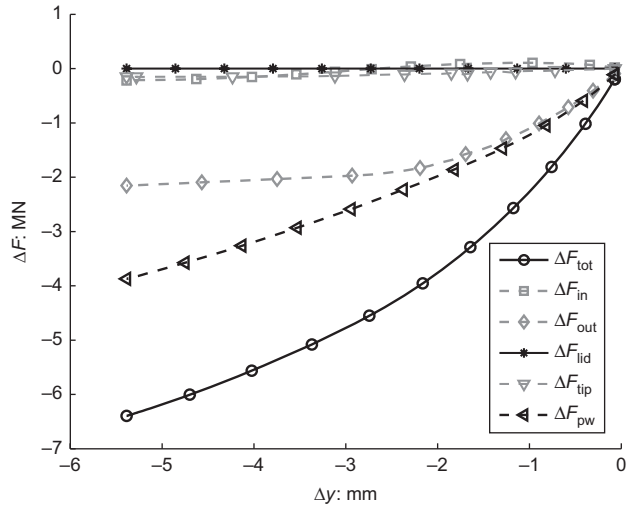

Fig. 17. Variations of global reaction components, traction partially drained simulation, $L = 6$ m, $k = 5 \times 10^{-12}$ m^2

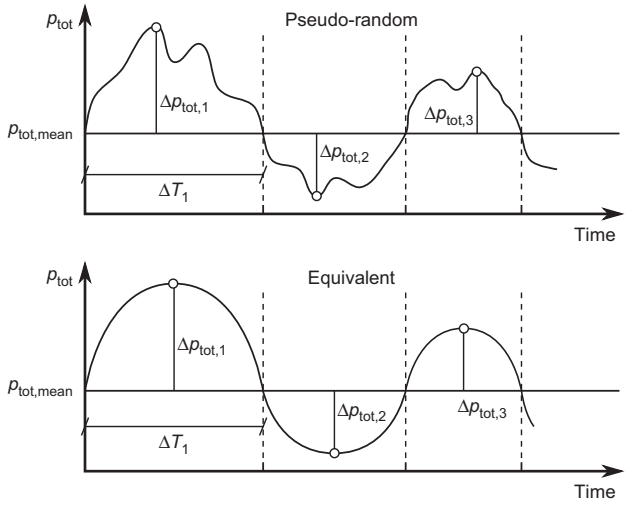

Fig. 18. Half-cycle analysis of load signal p_{tot}

Length of the caisson. The partially drained simulation of a longer suction caisson ($L = 6$ m) is provided in Fig. 17. For an identical displacement, the outer shear stress ΔF_{out} and the PWP ΔF_{pw} are increased with respect to the reference case. Assume the following linear increase of effective vertical stress σ'_v with depth y

$$\sigma'_v = (\gamma - \gamma_w)\, y + \sigma'_{v0} \tag{13}$$

where γ is the saturated specific weight of the soil, γ_w is the specific weight of water and σ'_{v0} is the initial effective vertical load at the top of the soil (equal to zero in this case). Therefore, the maximum shear load available is obtained by integrating equation (13) over the length L of the caisson

$$\begin{aligned} \Delta F_{out} &= -\pi D \int_0^L \mu K_0 \sigma'_v \, dy \\ &= -\pi D \mu K_0 \left[(\gamma - \gamma_w) \frac{L^2}{2} + \sigma'_{v0} L \right] \end{aligned} \tag{14}$$

where K_0 is the coefficient of earth pressure at rest. The non-linear dependence on L appears naturally. The analytical result in this case is equal to $\Delta F_{out} = -2{\cdot}33$ MN. The numerically computed value is lower since the uplifting process decreases the effective vertical stress within the soil. The maximum outer friction also increases slightly after -3 mm. Indeed, effective normal stresses within the interface increase due to the negative variation of PWP in the surrounding soil.

The PWP mobilised is also lower than in the reference case for a given displacement due to the modification of the drainage path. This demonstrates the multiple influence of this parameter.

CYCLIC LOADING

The loading of offshore wind turbines is inherently cyclic since it is mainly due to waves and wind. Therefore, the study of the cyclic behaviour of suction caissons is necessary to ensure their serviceability after a storm event.

Loading

The cyclic load is applied in three phases. The first consists in applying monotonically a mean load $p_{tot,mean} = 20$ kPa, in a drained fashion. This load corresponds to the weight of the wind turbine and the constant component of the storm. The second phase is the application of a cyclic loading around the mean load. Finally a 300 s consolidation phase at constant initial mean load is simulated in order to allow dissipation of PWP and to compute a final settlement.

The cyclic loading of the caisson originates from the effects of wind and waves acting on the offshore superstructure. A typical output of the analysis of a tripod superstructure to environmental loading is presented in Fig. 19 (top figure). It is termed pseudo-random since it results from a numerical analysis by specialised software. It corresponds to a storm sample including an extreme event, namely, the biggest load encountered by the superstructure during the storm. Only the vertical load applied by a leg of the superstructure is considered.

Within the pseudo-random signal, high-amplitude cycles alternate with the low-amplitude ones and the effect of each type of cycle is difficult to isolate. A half-cycle analysis (Byrne & Houlsby, 2002) is carried out to transform the pseudo-random signal into a sinusoidal equivalent one. A half-cycle is defined as the part of a signal between two successive crossings of its mean value, as shown in Fig. 18. A half period ΔT and a peak value Δp_{tot} are associated with each half-cycle. Therefore, an equivalent sinusoidal cycle of identical characteristics (ΔT, Δp_{tot}) can be reconstituted.

In this study, four types A_i of periods and amplitudes are identified in the pseudo-random load signal. They are supplied in Table 2. For each category A_i, N_i cycles are identified in the pseudo-random signal. These equivalent cycles are ordered into equivalent load signals, as depicted in Fig. 19. These signals mainly differ by the position of the extreme event, at the beginning, in the middle or at the end. A more detailed description of the method can be found in Cerfontaine (2014).

Results

Figure 20 presents a comparison between the first equivalent and the pseudo-random load signals. The variation of the total load, Δp_{tot}, around its mean value, $p_{tot,mean}$, is represented as well as the averaged PWP under the lid of the caisson, Δp_w. The full response signal is difficult to analyse due to the large number of cycles. Therefore, the envelope curve, that is the locus of local minima or maxima, is represented for both Δp_{tot} and Δp_w.

The tendency curve describes the long-term evolution of the PWP. If the process was totally reversible, the PWP

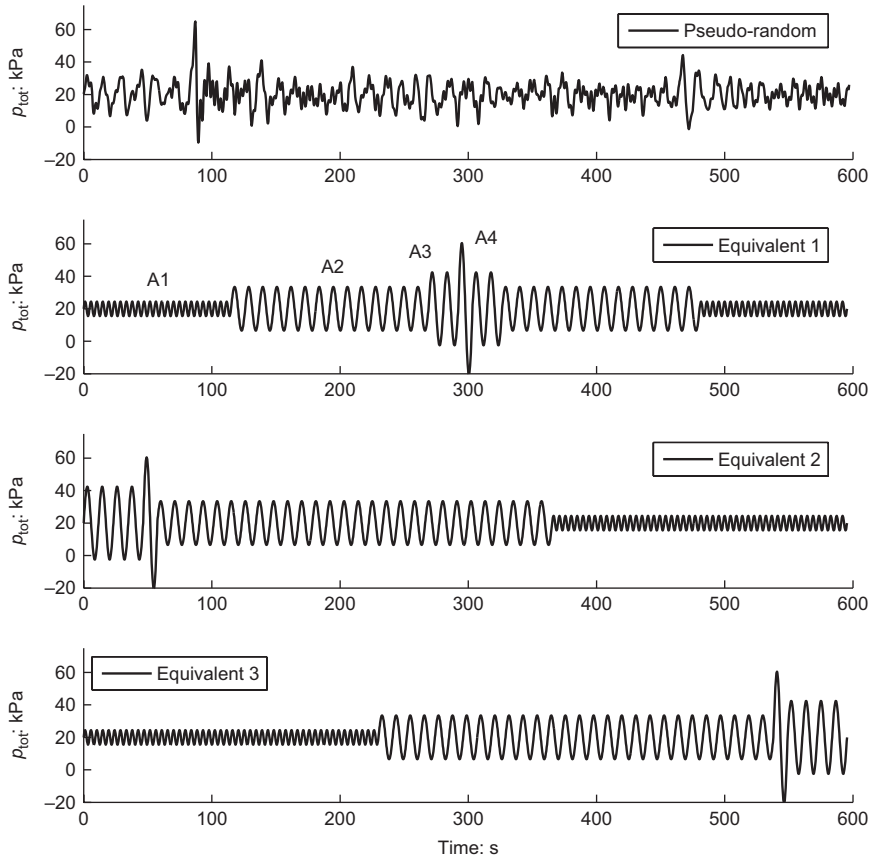

Fig. 19. Pseudo-random and equivalent cyclic load signals

Table 2. Number of equivalent cycles, associated amplitudes and periods

	A1	A2	A3	A4
Number of cycles	50	28	4	1
Δp_{tot}: kPa	4·5	13·5	22·5	40·5
T: s	4·6	11	11·6	11·1

should be equal to zero each time the cyclic amplitude Δp_{tot} is equal to zero. However, Δp_w is not equal to zero, denoting a non-recoverable part. The locus of all these non-recoverable parts describes the tendency response in Fig. 20.

It can be observed that the variation of PWP inside the caisson, Δp_w, is almost identical to the variation of the total load applied, Δp_{tot}. This is a consequence of the partially drained behaviour highlighted for monotonic simulations. A large part of the loading is sustained by a PWP variation which is hardly dissipated before the load reverses. Therefore, the cyclic effective amplitude applied to the solid skeleton of the soil surrounding the caisson is much lower than the total cyclic amplitude applied on the caisson. Consequently, this partially drained behaviour induces less stiffness degradation and settlement than a drained behaviour.

Both response signals present a tendency to PWP accumulation. Such an observation is classical in undrained laboratory experiments on soil samples (Seed & Lee, 1966; Alarcon-Guzman *et al.*, 1988) or in offshore engineering in general (Rahman *et al.*, 1977; Taiebat & Carter, 2000; Cuéllar *et al.*, 2014). This results from the plastic contractancy of the soil, implying excess PWP in partially drained conditions. In the upper graph of Fig. 20, it can be observed that a maximum accumulation arises after the extreme event. It is progressively dissipated afterwards during cycles of lower amplitudes.

The cyclic loading of suction caissons can be decomposed into two parallel consolidation processes. The first, referred to as short-term, consists of the immediate response of the soil to the variation of the applied load at the scale of a cycle. Variations of PWP are large since the load reverses before all PWP are dissipated. It is the origin of the 'suction effect'. The displacement varies accordingly and is mainly recoverable.

On the contrary, the second consolidation process arises from the progressive dissipation of the accumulated PWP and is referred to as long-term. It results from the plastic contractancy of the soil and is responsible of the non-recoverable settlement. Accumulation of deformation during cyclic loading is also a classical result, since it is linked to the accumulation of PWP.

The trend of settlement accumulation is computed similarly to the trend of PWP. It is the locus of the settlements measured each time the total load applied is equal to its mean value. Only this trend is represented since the full response signal is illegible due to the large number of cycles. The evolution of this permanent settlement under the top centre of the caisson is represented in Fig. 21. The maximum transient settlement encountered during the storm event (the global maximum) is also represented since it could affect serviceability.

Results presented converge to a similar final settlement, justifying the pertinence of the half-cycle analysis method for the elaboration of a load signal. However, there is a small divergence between them since the stress paths of material points are not identical for all load signals.

One of the advantages of such a load signal is the clarification of the effect of each batch of cycles. The low-amplitude cycles lead to almost no plastic deformation. This is quite

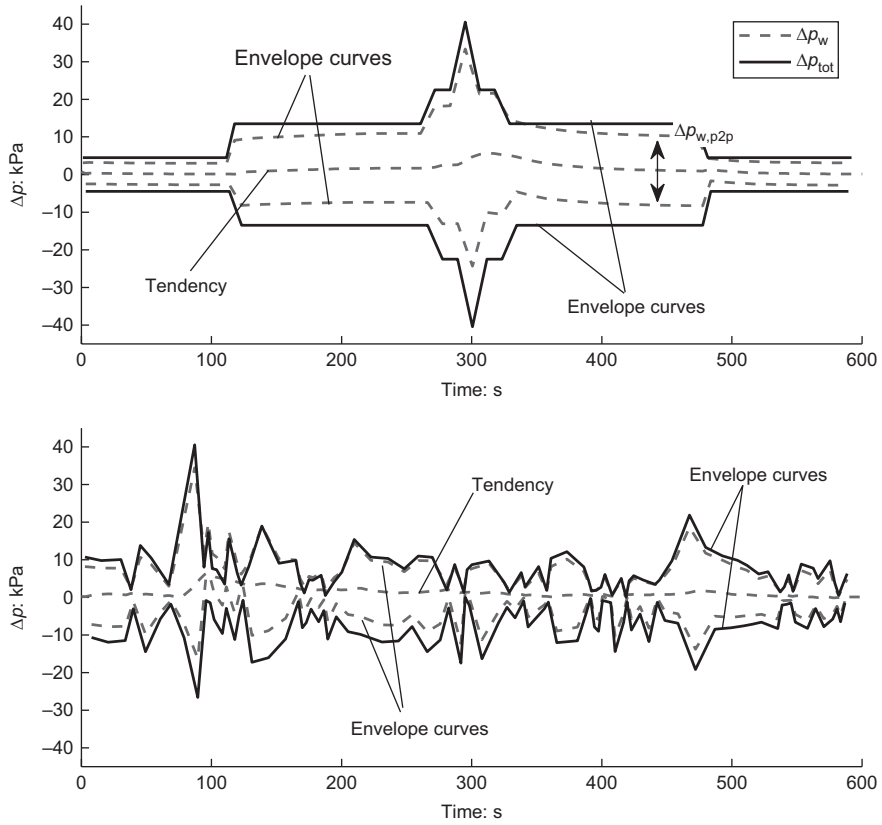

Fig. 20. Comparison of cyclic variation of total pressure applied on the lid Δp_{tot} and variation of mean pore pressure inside the caisson Δp_w for two load signals: equivalent 1 (up) and pseudo-random (down); total load applied to the caisson (solid black line), average PWP inside the caisson (dashed line)

clear in results corresponding to equivalent 3 load signal, but totally impossible to observe in the pseudo-random response. The second batch of cycles (A2) exhibits a clear tendency of settlement accumulation, which could be extrapolated to a larger number of cycles.

The asymptotic non-linear evolution of the settlement is due to the progressive dissipation of the accumulated PWP, which is maximum during the extreme event. Therefore, the sooner this event occurs, the sooner this asymptotic evolution starts.

For each class of equivalent cycles, described in Table 2, the difference between the upper and the lower envelope curves of PWP is almost constant. The variation of PWP between its minimum and maximum values over a cycle is termed $\Delta p_{w,p2p}$, as shown in Fig. 20.

It is shown in Kelly *et al.* (2006b) that the ratio between $\Delta p_{w,p2p}$ and the total variation of the load applied during this cycle, $2\Delta p_{tot}$, is constant with increasing load amplitude. This is also observed in the present work and depicted in Fig. 22. This ratio increases with the loading rate in Kelly *et al.* (2006b). Similarly, in this work, the ratio increases with a decreasing permeability.

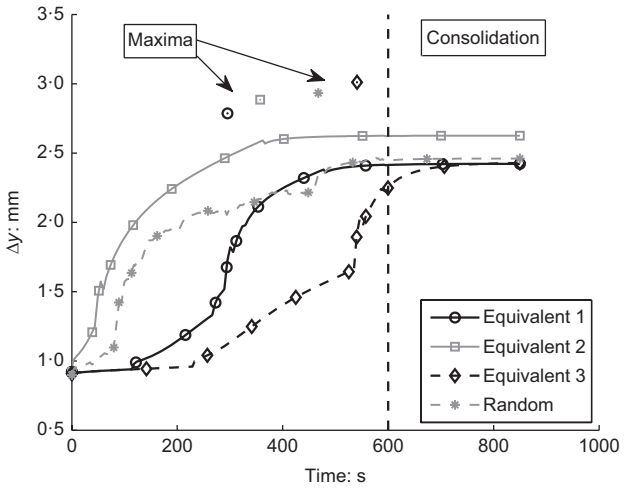

Fig. 21. Evolution of permanent displacement for four load signals (equivalent 1, equivalent 2, equivalent 3 and pseudo-random)

Influence of main parameters

The sensitivity of the results to permeability of the soil and soil–caisson friction coefficient is quite important to assess. Indeed, these parameters are not well mastered. Permeability of the soil is likely to be heterogeneous and difficult to quantify on site. The friction coefficient also depends on the installation process, the granulometry and the nature of the soil. The length of the caisson is one of the main parameters of the design. Therefore, the influence of these three parameters is investigated in the following. The reference simulation corresponds to the first equivalent (equivalent 1) load signal depicted in Figs 19–21.

Permeability. Permeability strongly influences the evolution of settlement with time. Fig. 23 illustrates two opposite effects of permeability. For permeability higher than the reference value ($k = 5 \times 10^{-12}$ m^2), the dissipation of PWP is faster. Therefore, the variations of effective stresses in the soil around are greater, inducing more settlement due to the rearrangement of solid grains. The highest permeability even leads to local failure of the soil, described hereafter. On the

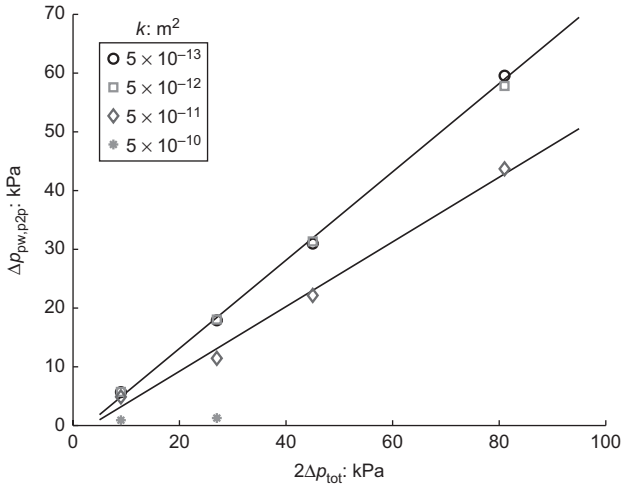

Fig. 22. Ratio between change of PWP $\Delta p_{w,p2p}$ (from minimum to maximum) and variation of total load applied $2\Delta p_{tot}$

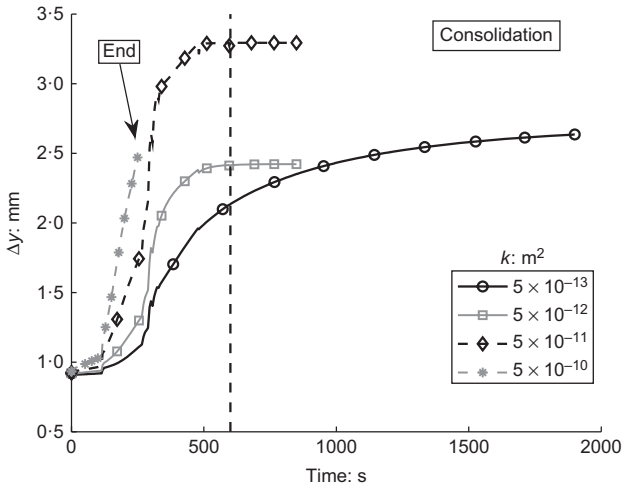

Fig. 23. Evolution of permanent displacement for four orders of magnitude of permeability, equivalent 1 load signal

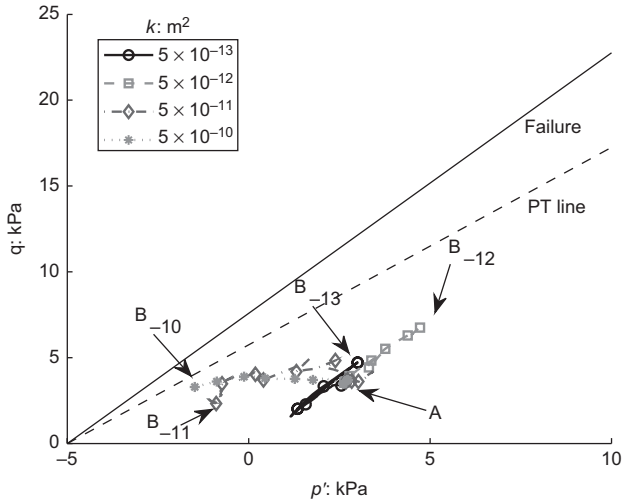

Fig. 24. Stress path of soil under centre of lid for three permeabilities: starting point A, end point B, equivalent 1 load signal

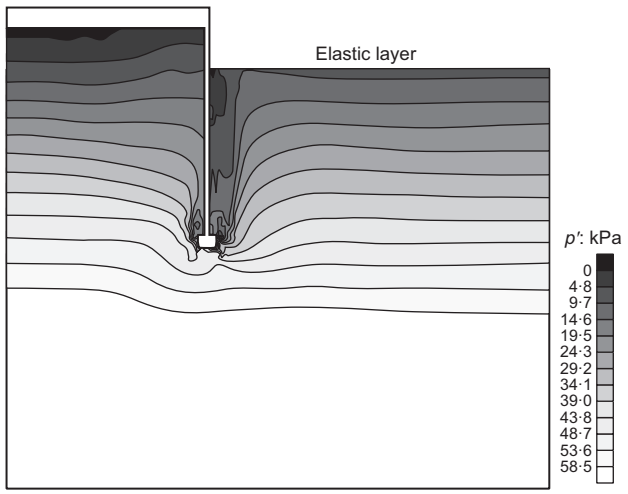

Fig. 25. Mean effective stress surrounding caisson at end of simulation, $k = 5 \times 10^{-10}$ m^2, equivalent 1 load signal

contrary, the lowest permeability case involves a lower settlement during the cyclic loading phase. However, the final settlement after consolidation is greater. This can be attributed to the highest PWP being accumulated during the loading, decreasing the stiffness of the material and increasing plasticity effects.

The stress path of a material point under the centre of the lid is compared for four permeabilities in Fig. 24. In the reference case the stress path tends towards an increasing p'. This evolution is correlated with small amplitude of effective stresses. The lowest permeability case first tends towards the decreasing p', as PWPs are accumulated. It reverts to increasing p' after consolidation.

On the contrary, the other results tend towards the origin of the axes and failure, termed 'initial liquefaction' in the literature (Seed & Lee, 1966). The very low confinement is illustrated in Fig. 25 in the case of the highest permeability case. The mean effective stress is strongly reduced, with respect to its initial value, under the lid and along the outer skirt, that is, in zones where the shear stress variations are high.

Friction coefficient. Friction phenomena play a crucial role in the resistance of suction caissons (Kourkoulis *et al.*, 2014; Thieken *et al.*, 2014) but also in the accumulation of settlement. Two cases are compared in Fig. 26, where the coefficient of friction is either equal to 0·0 or 0·5. In the first case, the soil plug is almost in oedometric conditions, as shown in Fig. 26(a). It settles while the outer surrounding soil remains almost unaffected.

In the other case, stress diffusion within the interface induces the settlement of a volume of soil in contact with the outer skirt of the caisson. This is marked in Fig. 26(b) by a gradient of vertical displacement next to the outer skirt of the caisson. This releases the load applied by the lid on the soil plug. Moreover the load is transferred through the interface to a soil at a higher confinement. This combined effect decreases the global settlement.

Caisson length. The influence of the caisson length on the cyclic loading of the caisson is presented in Fig. 27. The difference in settlement after the application of the initial monotonic load (time = 0 s) is not very high between $L = 4$ m and $L = 6$ m ($\sim 0{\cdot}2$ mm). However, at the end of the cyclic simulation, the increase of the settlement is three times greater for the smaller length.

For a lower length of the caisson, $L = 2$ m, the initial settlement of the caisson is much greater. Moreover, the accumulated settlement for the first cycles is very important

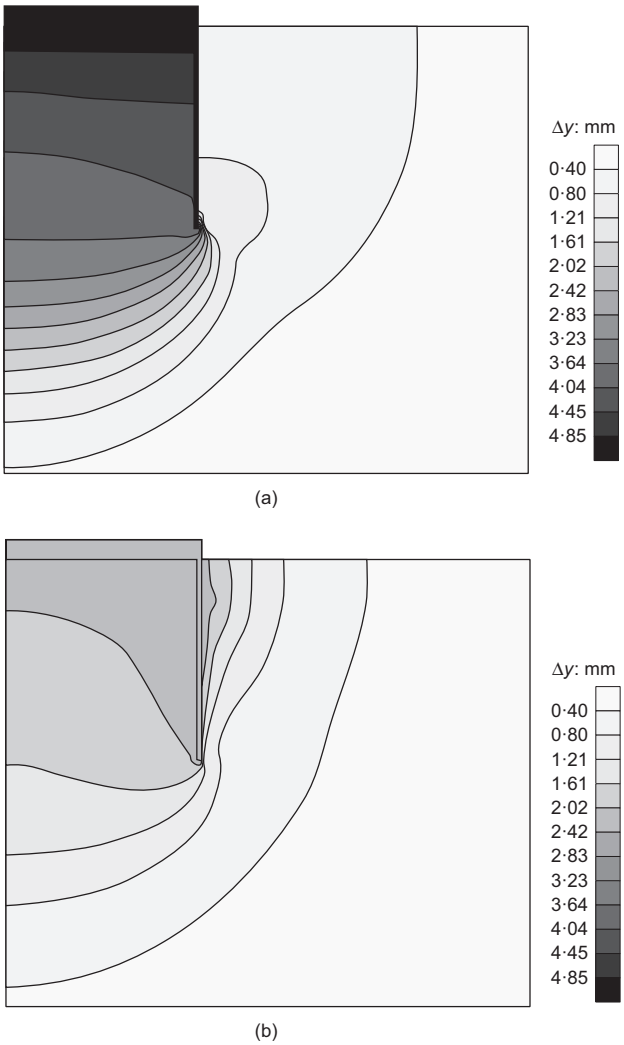

Fig. 26. Vertical displacement Δy at end of simulation, equivalent 1 load signal: (a) friction coefficient, $\mu = 0{\cdot}0$, maximum settlement 5·2 mm; (b) friction coefficient, $\mu = 0{\cdot}5$, maximum settlement 2·42 mm

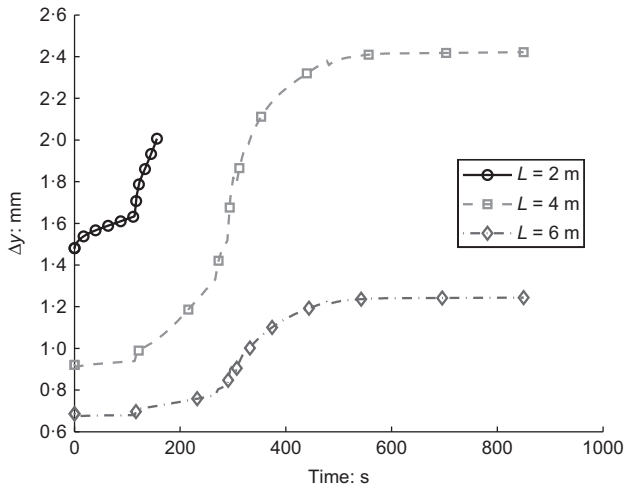

Fig. 27. Influence of length of caisson on vertical displacement, Δy, equivalent 1 load signal

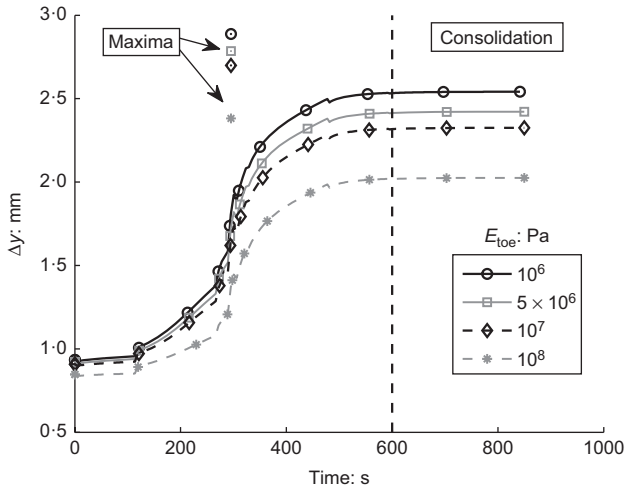

Fig. 28. Influence of elastic toe Young's modulus, equivalent 1 load signal

and the simulation finally stops due to the local failure of a material point.

The length of the caisson increases the surface over which friction can be mobilised. It also diffuses shear stresses at a greater depth where confinement and resistance of the soil are greater. Moreover, the drainage path of the soil plug is increased. For all these reasons, the amplitudes of effective stresses transferred to the soil are lower, reducing the final settlement reached. An increase of 50% of the length induces a reduction of 66% of the accumulated settlement.

Young's modulus of the elastic toe. The influence of the Young's modulus of the elastic toe is illustrated in Fig. 28. It illustrates that the choice of this parameter should be done carefully. Indeed the skirt acts as a bearing for the lid. However, this bearing is not a fixed point but has a stiffness. This stiffness is altered by modifying the properties of the elastic toe. Therefore, the distribution between the different components of reaction also differs.

Decreasing the elastic modulus reduces the stiffness of the bearing. Therefore, the lid component ΔF_{lid} is increased as well as the shear stress components ΔF_{in} and ΔF_{out}. These loads are transferred from the caisson to the soil in a zone where the confinement and resistance are lower than under the tip. In conclusion, the lower the Young's modulus is, the larger is the settlement accumulated at the end of the load signal. However, it was determined during the choice of the Young's modulus that it should lie between 10^6 Pa and 10^7 Pa. For this range, the final settlement reached does not vary significantly from the reference case.

Cyclic diagram

In this section a cyclic diagram is proposed for the reference suction caisson. It relates the increment of settlement accumulated after a given storm event, that is, the difference between the settlement at the end and at the beginning of the cyclic loading. The reference equivalent 1 load signal is shifted to allow the simulation of signals with varying mean load, $p_{\text{tot,mean}}$. It is also scaled to obtain a different maximum cyclic amplitude, Δp_{tot}. These variables are described in Fig. 29. The number and periods of each cycle type remain unchanged. The final cyclic diagram represents the accumulation of settlement after the storm event and is based on 32 combinations of mean and cyclic loads ($p_{\text{tot,mean}}$, Δp_{tot}). It must be kept in mind that this example is limited to the parameters of the reference case presented before.

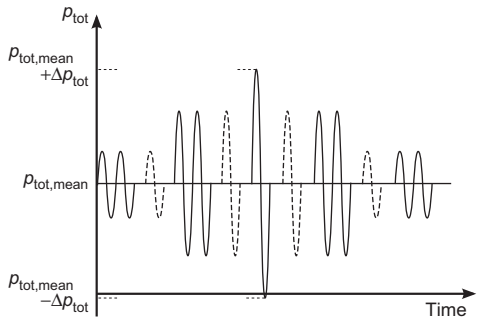

Fig. 29. Short storm signal scaled to correspond to a combination of ($p_{tot,mean}$, Δp_{tot})

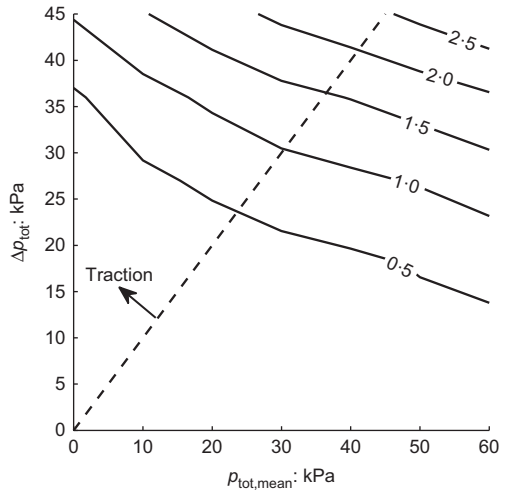

Fig. 30. Increment of vertical displacement Δy (mm) after a storm loading for a combination of mean load, $p_{tot,mean}$, and maximum cyclic amplitude, Δp_{tot}; geometry and parameters correspond to the reference case

The main purpose of such a diagram is to assess the effect of a given storm event on the system of foundations. It is a tool of pre-design, avoiding the necessity of running complex simulations. Most of the time, such diagrams relate a combination of loading to the number of cycles to failure (Andersen *et al.*, 2013). However, failure is not easy to define since it could correspond to a global failure of the soil or an excessive settlement. Moreover, local failure should be overcome. Therefore, the proposed cyclic diagram describes the accumulation of settlement for a given storm event. It is a tool assessing serviceability rather than failure.

Results are presented in Fig. 30. During simulations, traction loads were encountered at least during the extreme event, since $p_{tot,cycl} \geq p_{tot,mean}$. However, this does not lead to failure of the caisson. It can be observed that increasing the mean load involves less settlement accumulation than increasing the cyclic amplitude. Moreover, a combination of zero mean load and a cyclic amplitude of 37 kPa produces the same settlement as a mean load of 60 kPa and a cyclic load of 15 kPa. This highlights that the maximum amplitude value alone is not a correct indicator of the settlement increment.

CONCLUSIONS

Suction caissons represent an interesting competitive alternative to other types of foundations for offshore wind turbines. However, their behaviour upon traction and cyclic loading is not entirely mastered and simplified methods for design should still be elaborated. This paper presents the results of monotonic and cyclic loading of a suction caisson embedded in dense sand.

Upon traction, the main mechanism of reaction is the friction progressively mobilised along the skirt of the caisson. It is mobilised inside and outside the caisson in drained conditions (low pull rate). Upon high rate of loading, a consolidation process takes place, generating over- or under-pressures, respectively, with compression or traction loads. The differential of pressure between inside and outside the caisson creates a suction effect, increasing the resistance of the caisson in both traction and compression. It is of greater importance in traction than in compression.

The suction phenomenon is the cornerstone of suction caisson behaviour and is affected by many of the parameters studied in this work (constitutive law, permeability of the soil, length of the caisson). The importance of friction and loss of contact justifies the use of interface elements. Therefore, drainage conditions mainly influence the design procedure, since all mechanisms are not activated in all cases. Moreover, the vertical displacements necessary to fully activate a mechanism also differ.

The cyclic loading of suction caissons is mainly partially drained. Therefore, the major part of the load variation is sustained by positive or negative variations of PWP within the soil inside the caisson and around it. The principal consequence is a low loading of the solid skeleton of the soil. All simulations present an accumulation of settlement during the cyclic loading of the caisson. However, this settlement is reduced with respect to a purely drained behaviour. The influence of the main parameters is also assessed, highlighting the crucial role of friction and drainage conditions.

An example of a cyclic diagram for pre-design of suction caisson foundations is elaborated. It relates the average and cyclic components of the loading to a final settlement for a given storm event. It could assist the quick pre-design of such foundation systems.

Numerical modelling of suction caissons under cyclic loading is a challenging task but entails interesting perspectives. The possibilities of improving the results are numerous and, among them, the implementation of a constitutive law describing the evolution of the friction angle of the soil–caisson interface should be interesting (Liu & Ling, 2008).

The accurate description of the mechanisms of resistance could lead naturally to a spring–dashpot macro-element, describing the behaviour of the caisson. This has already been done in Senders (2008), but the definition of the different parameters is still an issue. Moreover, the modelling of settlement accumulation upon cyclic loading requires the elaboration of a more complex non-linear law for the springs.

NOTATION

D	diameter of caisson (m)
E	Young's modulus
g_N	gap opening between two sides of an interface element (m)
f_{wl}	longitudinal water flow
f_{wt}	transverse water flow
K_0	coefficient of earth pressure at rest
K_N	penalty coefficient (normal) (N/m^3)
K_T	penalty coefficient (tangential) (N/m^3)
k	permeability (m^2)
k_l	longitudinal permeability
L	length of caisson (m)
M'	aperture of the surface
p'	mean effective stress (Pa)
p_c	cohesion shift on hydrostatic axis (Pa)
p'_N	effective contact stress (Pa)
p_{tot}	total pressure applied on top surface of caisson (Pa)

$p_{tot,mean}$ mean value of total pressure applied on top surface of caisson during cyclic loading (Pa)
p_w pore water pressure (Pa)
q invariant of deviatoric stress (Pa)
T_w transversal conductivity
y depth
$\boldsymbol{\alpha}$ back-stress tensor
γ saturated specific weight of the soil
γ_w specific weight of water
ΔF_{in} total load mobilised by shearing within inner interface (N)
ΔF_{lid} total effective contact load under lid (N)
ΔF_{ou} total load mobilised by shearing within outer interface (N)
ΔF_{pw} total load due to difference of water pressure under lid (N)
ΔF_{tip} total load under tip (N)
ΔF_{tot} total load applied at top of caisson (N)
Δp_{tot} variation of total pressure applied on top of caisson (N)
Δp_w variation of pore water pressure (N)
Δy vertical displacement under centre of caisson (m)
$\dot{\varepsilon}_v^p$ plastic component of the variation of volumetric strains
μ friction coefficient
μ_w dynamic viscosity of water
ρ_w specific mass of the fluid
$\boldsymbol{\sigma}'$ effective stress tensor (Pa)
σ'_v vertical stress
σ'_{v0} initial effective vertical load at the top of the soil
τ shear stress
τ_{max} maximum shear stress

REFERENCES

Achmus, M., Akdag, C. T. & Thieken, K. (2013). Load-bearing behavior of suction bucket foundations in sand. *Appl. Ocean Res.* **43**, 157–165, http://dx.doi.org/10.1016/j.apor.2013.09.001.

Alarcon-Guzman, A., Leonards, G. & Chameau, J. (1988). Undrained monotonic and cyclic strength of sands. *J. Geotech. Engng* **114**, No. 10, 1089–1109.

Andersen, K., Jostad, H. & Dyvik, R. (2008). Penetration resistance of offshore skirted foundations and anchors in dense sand. *J. Geotech. Geoenviron. Engng* **134**, No. 1, 106–116.

Andersen, K., Puech, A. & Jardine, R. (2013). Cyclic resistant geotechnical design and parameter selection for offshore engineering and other applications. In *Proceedings of TC 209 workshop – 18th ICSMGE* (ed. A. Peuch), pp. 9–44. Paris, France: Presses des Ponts.

Byrne, B. & Houlsby, G. (2002). Experimental investigations of response of suction caissons to transient vertical loading. *J. Geotech. Geoenviron. Engng* **128**, No. 11, 926–939.

Byrne, B. & Houlsby, G. (2003). Foundations for offshore wind turbines. *Phil. Trans. Ser. A: Math., Phys., Engng Sci.* **361**, No. 1813, 2909–2930.

Byrne, B. & Houlsby, G. (2004). Experimental investigations of the response of suction caissons to transient combined loading. *J. Geotech. Geoenviron. Engng* **130**, No. March, 240–253.

Cerfontaine, B. (2014). *The cyclic behaviour of sand, from the Prevost model to offshore geotechnics*. PhD thesis, University of Liège, Liège, Belgium.

Cerfontaine, B., Levasseur, S., Collin, F. & Charlier, R. (2014). Axisymmetric transient modelling of a suction caisson in dense sand. In *Proceedings of the 8th European conference on numerical methods in geotechnical engineering, NUMGE 2014* (eds M. Hicks, R. Brinkgreve and A. Rohe), vol. 2, pp. 1243–1248. London, UK: Taylor and Francis.

Cerfontaine, B., Collin, F. & Charlier, R. (2015a). Vertical transient loading of a suction caisson in dense sand. *Computer methods and recent advances in geomechanics – Proceedings of the 14th international conference of the International Association for Computer Methods and Recent Advances in Geomechanics, IACMAG 2014* (eds F. Oka, A. Murakami, R. Uzuoka and S. Kimoto), pp. 929–934. London, UK: Taylor and Francis.

Cerfontaine, B., Dieudonne, A., Radu, J., Collin, F. & Charlier, R. (2015b). 3d zero-thickness coupled interface finite element: formulation and application. *Comput. Geotech.* **69**, 124–140, http://dx.doi.org/10.1016/j.compgeo.2015.04.016.

Corbetta, G., Miloradovic, T., Pineda, I., Azau, S., Moccia, J. & Wilkes, J. (2014). *Wind in power, 2013 European statistics*, Technical report. Brussels, Belgium: European Wind Energy Association.

Cuéllar, P., Mira, P., Pastor, M., Fernández Merodo, J., Baeßler, M. & Rücker, W. (2014). A numerical model for the transient analysis of offshore foundations under cyclic loading. *Comput. Geotech.* **59**, 75–86, http://dx.doi.org/10.1016/j.compgeo.2014.02.005.

Dafalias, Y. & Popov, E. (1975). A model of nonlinearly hardening materials for complex loading. *Acta Mechanica* **21**, No. 3, 173–192.

Gao, Y., Qiu, Y., Li, B., Li, D., Sha, C. & Zheng, X. (2013). Experimental studies on the anti-uplift behavior of the suction caissons in sand. *Appl. Ocean Res.* **43**, 37–45, http://dx.doi.org/10.1016/j.apor.2013.08.001.

Gens, A., Carol, I. & Alonso, E. (1988). An interface element formulation for the analysis of soil reinforcement interaction. *Comput. Geotech.* **7**, No. 1–2, 133–151.

Gerard, P., Charlier, R., Chambon, R. & Collin, F. (2008). Influence of evaporation and seepage on the convergence of a ventilated cavity. *Water Resources Res.* **44**, No. 5, W00C02.

Goodman, L., Lee, C. & Walker, F. (1961). The feasibility of vacuum anchorage in soil. *Géotechnique* **11**, No. 4, 356–359, http://dx.doi.org/10.1680/geot.1961.11.4.356.

Goodman, R., Taylor, R. & Brekke, T. (1968). A model for the mechanics of jointed rock. *J. Soil Mech. Found. Div.* **94**, 637–659.

Habraken, A., Cescotto, S. & Banning, Q. (1998). Contact between deformable solids: the fully coupled approach. *Math. Comput. Modelling* **28**, No. 4, 153–169.

Houlsby, G. & Byrne, B. (2005). Design procedures for installation of suction caissons in sand. *Proc. Instn Civ. Engrs – Geotech. Engng* **158**, No. 3, 135–144.

Houlsby, G., Ibsen, L. & Byrne, B. (2005a). Suction caissons for wind turbines. In *Frontiers in offshore geotechnics: IS-FOG 2005* (eds S. Gourvenec and M. Cassidy), pp. 75–94. London, UK: Taylor and Francis.

Houlsby, G., Kelly, R. & Byrne, B. (2005b). The tensile capacity of suction caissons in sand under rapid loading. In *Frontiers in offshore geotechnics: IS-FOG 2005* (eds S. Gourvenec and M. Cassidy), pp. 405–410. London, UK: Taylor and Francis.

Houlsby, G., Kelly, R., Huxtable, J. & Byrne, B. (2006). Field trials of suction caissons in sand for offshore wind turbine foundations. *Géotechnique* **56**, No. 1, 3–10, http://dx.doi.org/10.1680/geot.2006.56.1.3.

Hyodo, M., Hyde, A., Aramaki, N. & Nakata, Y. (2002). Undrained monotonic and cyclic shear behaviour of sand under low and high confining stress. *Soils Found.* **42**, No. 3, 63–76.

Ibsen, L. & Jacobsen, F. (1996). Lund sand no. 0, Technical report. Aalborg University, Aalborg, Denmark.

Ishihara, K. (1996). *Soil behaviour in earthquake geotechnics*. Oxford, UK: Oxford University Press.

Iskander, M., El-gharbawy, S. & Olson, R. (2002). Performance of suction caissons in sand and clay. *Can. Geotech. J.* **584**, No. 3, 576–584.

Kelly, R., Houlsby, G. & Byrne, B. (2006a). A comparison of field and laboratory tests of caisson foundations in sand and clay. *Géotechnique* **56**, No. 9, 617–626, http://dx.doi.org/10.1680/geot.2006.56.9.617.

Kelly, R. B., Houlsby, G. T. & Byrne, B. W. (2006b). Transient vertical loading of model suction caissons in a pressure chamber. *Géotechnique* **56**, No. 10, 665–675, http://dx.doi.org/10.1680/geot.2006.56.10.665.

Kourkoulis, R., Lekkakus, P., Gelagoti, F. & Kaynia, A. (2014). Suction caisson foundations for offshore wind turbines subjected to wave and earthquake loading: effect of soil–foundation interface. *Géotechnique* **64**, No. 3, 171–185, http://dx.doi.org/10.1680/geot.12.P.179.

Lehane, B., Elkhatib, S. & Terzaghi, S. (2014). Extraction of suction caissons in sand. *Géotechnique* **64**, No. 9, 735–739, http://dx.doi.org/10.1680/geot.14.T.011.

Liu, H. & Ling, H. (2008). Constitutive description of interface behavior including cyclic loading and particle breakage within the framework of critical state soil mechanics. *Int. J. Numer. Analyt. Methods Geomech.* **32**, No. 12, 1495–1514.

Prevost, J. (1977). Mathematical modelling of monotonic and cyclic undrained clay behaviour. *Int. J. Numer. Analyt. Methods Geomech.* **1**, No. 2, 195–216.

Prevost, J. (1985). A simple plasticity theory for frictional cohesionless soils. *Int. J. Soil Dynamics Earthquake Engng* **4**, No. 1, 9–17.

Rahman, M., Seed, H. & Booker, J. (1977). Pore pressure development under offshore gravity structures. *J. Geotech. Engng Div.* **103**, No. 12, 1419–1436.

Seed, B. & Lee, K. (1966). Liquefaction of saturated sands during cyclic loading. *J. Soil Mech. Found. Div.* **92**, No. 6, 105–134.

Segura, J. & Carol, I. (2008). Coupled HM analysis using zero-thickness interface elements with double nodes. Part i: theoretical model. *Int. J. Numer. Analyt. Methods Geomech.* **32**, No. 18, 2083–2101.

Senders, M. (2008). *Suction caissons in sand as tripod foundations for offshore wind turbines*. PhD thesis, University of Western Australia, Crawley, WA, Australia.

Senders, M. & Randolph, M. (2009). CPT-based method for the installation of suction caissons in sand. *J. Geotech. Geoenviron. Engng* **135**, No. 1, 14–25.

Senpere, D. & Auvergne, G. (1982). Suction anchor piles – a proven alternative to driving or drilling. *Proceedings of the offshore technology conference*, Houston TX, paper OTC 4206.

Taiebat, H. & Carter, J. (2000). A semi-empirical method for the liquefaction analysis of offshore foundations. *Int. J. Numer. Analyt. Methods Geomech.* **24**, No. 13, 991–1011.

Thieken, K., Achmus, M. & Schröder, C. (2014). On the behavior of suction buckets in sand under tensile loads. *Comput. Geotech.* **60**, 88–100, http://dx.doi.org/10.1016/j.compgeo.2014.04.004.

Tjelta, T., Aas, P., Hermstad, J. & Andenaes, E. (1990). The skirt piled Gullfaks C platform installation. *Proceedings of the offshore technology conference*, Houston TX, paper OTC 6473.

Tran, M. (2005). *Installation of suction caissons in dense sand and the influence of silt and cemented layers.* PhD thesis, The University of Sydney, Sydney, NSW, Australia.

Wriggers, P. (2006). *Computational contact mechanics*, 2nd edn. Chichester, UK: Wiley.

Yang, Z., Elgamal, A. & Parra, E. (2003). Computational model for cyclic mobility and associated shear deformation. *J. Geotech. Geoenviron. Engng* **129**, No. 12, 1119–1127.

Zhu, B., Byrne, B. & Houlsby, G. (2013). Long-term lateral cyclic response of suction caisson foundations in sand. *J. Geotech. Geoenviron. Engng* **139**, No. 1, 73–83, http://dx.doi.org/10.1061/(ASCE)GT.1943-5606.0000738.